Folding model analysis of the excitation of low-lying states and the high energy octupole resonance in ^{116}Sn by 240 MeV α scattering

H. L. Clark, Y.-W. Lui, and D. H. Youngblood
Cyclotron Institute, Texas A&M University, College Station, Texas 77843
(Received 23 October 1997)

The sum rule strength of the high energy octupole resonance (HEOR) and the transition rates of low-lying 2^+ and 3^- states of ^{116}Sn, excited by 240 MeV α scattering, have been determined from deformed potential and folding model analyses. Deformed potential cross sections for both the low-lying 3^- state and the HEOR are greater than folding cross sections by a factor of 1.18. The high energy octupole resonance was found to exhaust (70 ± 15)% and (83 ± 15)% of the $E3$ energy-weighted sum rule from the two analyses, respectively. The data for the low-lying states are fit well by the calculations made with both models using electromagnetic values for the transition rates. Optical-model parameters were obtained from fits to elastic scattering data. The differential cross sections for the elastic scattering and inelastic scattering exciting the low-lying 2^+ and 3^- states in ^{116}Sn were measured over the angle range from $\theta_{\text{c.m.}}=1.6°$ to 35.2°. [S0556-2813(98)00306-9]

PACS number(s): 24.30.Cz, 21.60.Ev, 25.55.Ci, 27.60.+j

I. INTRODUCTION

In a previous work, we used the deformed potential (DP) model to analyze the scattering of 240 MeV α particles on ^{116}Sn and found that the isoscalar high energy octupole resonance (HEOR) exhausted (67 ± 10)% [1] of the $E3$ energy-weighted sum rule (EWSR). However, it has been shown from analyses of ^{17}O scattering on several nuclei (including ^{120}Sn) [2] that the DP model overpredicts the transition strength of the low-lying 3^- state. Recently, similar conclusions were drawn in a study of 240 MeV α scattering on ^{58}Ni where the cross sections calculated for the 4.485 MeV 3^- state with the DP model were about 50% too high, while cross sections obtained with the folding model agreed with the data using the $B(E3)$ value from electromagnetic measurements [3]. These results suggest that the sum rule strength we obtained for the HEOR in ^{116}Sn might be low since the expressions for the transition operators of the low-lying 3^- state and the HEOR are the same.

In this paper, we apply the folding model to the HEOR data for ^{116}Sn reported in Ref. [1]. Optical potentials used in the analyses were determined by fitting newly measured elastic data. The data extended over the range of $1.6° \leqslant \theta_{\text{c.m.}} \leqslant 35.2°$ and displayed the beginning of rainbow scattering. The differential cross sections for the low-lying 2^+ state at 1.29 MeV and 3^- state at 2.27 MeV were also extracted from the data. The folding model was tested by calculating cross sections for these states.

II. OPTICAL AND TRANSITION MODELS

In the DP model, excitations of the nucleus with multipolarity $l \geqslant 2$ are characterized by a transition potential whose shape is independent of l [4]:

$$G_l^{\text{DP}}(r) = -\delta_l^U \frac{dU(r)}{dr}, \tag{1}$$

where $U(r)=V(r)+iW(r)$ is the complex optical model of the usual Woods-Saxon form (CWS) and δ_l^U is the potential deformation length (with $\delta_l^v=\delta_l^w$) where the matter and potential deformation lengths are equal, $\delta_l^m=\delta_l^U$.

A more fundamental way to describe inelastic scattering is to obtain optical and transition potentials from folding an effective nucleon-nucleon interaction over the density distributions of the projectile and nucleus. For α particle scattering, the method can be simplified by using an effective α-nucleon interaction and integrating over the target density only. Using a Gaussian shaped α-nucleon interaction [5], the complex optical potential can then be written as

$$U(r) = -(v+iw)\int \rho(r')e^{(-s^2/t^2)}d\tau, \tag{2}$$

where v and w are optical potentials whose strengths are determined by fitting elastic scattering, $s=|\vec{r}-\vec{r}'|$ is the distance between a target nucleon and the center of mass of the α particle, and t is a range parameter which is fixed at 1.94 fm [6]. The ground state density of the target nucleus is expressed as

$$\rho(r') = \rho_0(1+e^{[(r'-c)/a]})^{-1}, \tag{3}$$

where the Fermi-model density parameters for ^{116}Sn are $c=5.433$ fm and $a=0.515$ fm [7]. The value for c was interpolated from the values of ^{112}Sn and ^{118}Sn of Ref. [7].

For a collective vibration of the nucleus, of multipole $l \geqslant 2$, the transition density can be expressed as [8]

$$g_l(r') = -\delta_l^m \frac{d\rho(r')}{dr'}, \tag{4}$$

where δ_l^m is the matter deformation length. For α particle scattering, the transition potential can then determined by folding the α-nucleon interaction over the transition density

$$G_l^{\text{folding}}(r) = -(v+iw)\sqrt{4\pi/(2l+1)} \times \int g_l(r')e^{(-s^2/t^2)}Y_0^l d\tau. \tag{5}$$

For α particle energies which demonstrate the rainbow effect in large angle elastic scattering ($E_\alpha \geq 100$ MeV), it has been found necessary to replace the complex part of Eq. (2) with a Woods-Saxon form [3]. The need for this suggests that the real and imaginary parts of the interaction have different radial dependencies. The potential is then

$$U(r) = -v \int \rho(r') e^{(-s^2/t^2)} d\tau - iW(1+e^{(r-R_w)/a_w})^{-1}, \tag{6}$$

where v, W, R_w, and a_w are parameters determined by fitting to elastic scattering. Equation (6) is referred to as a density-independent folding with imaginary Woods-Saxon (DIWS) optical model. The transition potential also changes as the imaginary term is replaced with a deformed potential form

$$G_l^{\mathrm{DIWS}}(r) = -v\sqrt{4\pi/(2l+1)} \int g_l(r') e^{(-s^2/t^2)} Y_0^l d\tau + i\delta_l^w \frac{W}{a_w} (1+e^{(r-R_w)/a_w})^{-2}, \tag{7}$$

where $\delta_l^W = \delta_l^m$.

At these energies ($E_\alpha \geq 100$ MeV), the projectile-nucleus collisions are no longer only peripheral and the α particle penetrates into the interior of the target. Analyses have shown [9] that the optical model expressed in Eq. (6) cannot describe elastic scattering both in the diffractive and rainbow angle regions. In this form, the strength of interaction for interior collisions may be overpredicted. To correct for this effect, the alpha-nucleon interaction can be multiplied by a density-dependence factor which reduces the strength of potential in the interior of the nucleus while leaving the strength of the potential at the surface unchanged. We adopt the form used by Satchler [3] which is parametrized as $f(\rho) = 1 - \alpha\rho(r')^\beta$, where $\alpha = 1.9\ \mathrm{fm}^2$ (with a corresponding range parameter of $t = 1.88$ fm) and $\beta = \frac{2}{3}$. This optical model is called density-dependent folding with imaginary Woods-Saxon (DDWS). For optical potentials which are obtained with density dependence, the α-nucleon interaction of the transition potential is also multiplied by a correction factor $f'(\rho) = 1 - \alpha(1+\beta)\rho(r')^\beta$, which has the effect of further reducing the strength of interaction in the interior of the nucleus [3].

III. SUM RULES AND TRANSITION RATES

For isoscalar transitions, the proton deformation length corresponding to 100% of the electric sum rule limit for multipoles of $l \geq 2$, is [10]

$$\delta_l^p = \sqrt{\frac{2\pi\hbar^2}{mAE_x} \frac{l(2l+1)^2}{(l+2)^2} \frac{\langle r^{2l-2}\rangle}{\langle r^{l-1}\rangle^2}}, \tag{8}$$

where m is the proton mass, A is the target nucleon number, E_x is the excitation energy of the state, and $\langle r^{2l-2}\rangle$ and $\langle r^{l-1}\rangle$ are radial moments evaluated over the proton distribution. If we assume the proton and neutron distributions and deformation lengths to be equal, $\delta_l^p = \delta_l^n \equiv \delta_l^m$, then the transition rate and deformation length are related by [4]

$$B(El) = \left(\frac{1}{4\pi} \delta_l^m Z(l+2)\langle r^{l-1}\rangle \right)^2, \tag{9}$$

where Z is the proton number of the nucleus and $\langle r^{l-1}\rangle$ is the radial moment of the mass distribution.

IV. EXPERIMENTAL TECHNIQUE

The following section discusses the experimental technique used to obtain the elastic scattering differential cross section and inelastic scattering differential cross sections for the low-lying 2^+ and 3^- states. The HEOR data is from Ref. [1].

Beams of 240 MeV α particles from the Texas A&M K500 superconducting cyclotron bombarded a self-supporting 11.44 mg/cm^2 Sn foil enriched to 95% in ^{116}Sn in the target chamber of the multipole-dipole-multipole spectrometer (MDM) [11]. The beam was delivered to the MDM through a beam analysis system [12], to remove halo and improve momentum resolution, and was stopped either beside the solid angle defining slits or on a Faraday cup inside the target chamber. Elastically scattered α particles and inelastically scattered α particles down to $\sim$200 MeV were detected by a newly constructed detector at the focal plane of the MDM. The detector consisted of four 60 cm long proportional counters to measure x position and θ, an ionization chamber to measure ΔE, and a scintillator to measure E and to provide a fast trigger. The angle ϕ was not measured. The principles of operation are similar to the detector in Ref. [13].

Data were taken at spectrometer angles of 3.5°, 5°, 7°, 9°, 11°, 13°, 16°, 19°, 22°, 26°, 29°, and 32° with a spectrometer acceptance of $\Delta\theta = 4.0°$ and $\Delta\phi = \pm 0.8°$. In the analysis, software cuts on θ were applied to divide each data set into ten angle bins, each corresponding to $\Delta\theta \approx 0.4°$. Since ϕ was not measured by the detector, the average angle for each bin was determined by averaging over the height of the solid angle defining slit and the width of the angle bin. For each angle bin, the elastic and inelastic scattering peak positions, widths, and cross sections were extracted by integration or by a Gaussian fitting routine. The elastic and inelastic scattering differential cross sections obtained are plotted versus average center-of-mass angle in Figs. 1 and 2. The error bars represent the combined uncertainty from statistical and systematic error summed in quadrature. Absolute cross sections were obtained from the combination of charge integration, target thickness, solid angle, and dead time. Data from a monitor detector, fixed at $\theta_{\mathrm{lab}} = 20°$, were used to verify the normalizations between the different data sets across the entire angular range. The elastic and inelastic cross sections agreed within the errors with those of Ref. [14] who measured scattering out to $\theta_{\mathrm{lab}} \sim 16°$.

V. DATA ANALYSIS AND DISCUSSION

Optical-model calculations were carried out using the coupled-channels program PTOLEMY [15]. Since PTOLEMY calculates all kinematics nonrelativistically, corrections to the projectile mass and lab energy were made to achieve a proper relativistic calculation [16]. Form factors for the folded potentials were calculated externally by numerical in-

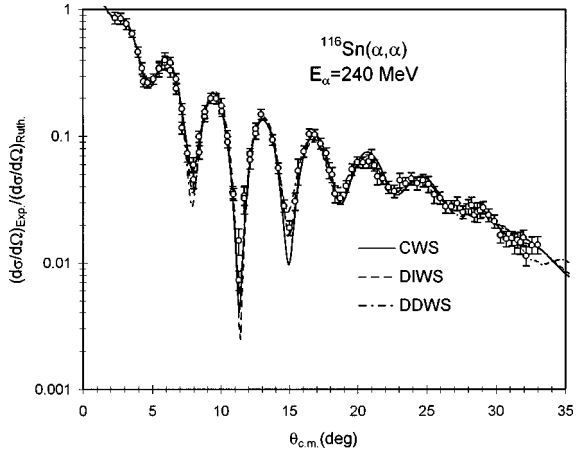

FIG. 1. Angular distribution of the ratio of elastic scattering differential cross section to Rutherford scattering for 240 MeV α particles on ^{116}Sn plotted versus average center-of-mass angle. The error bars represent the combined uncertainty from statistical and systematic error summed in quadrature. The solid, dashed, and dashed-dot lines are from complex Woods-Saxon, density-independent folding with imaginary Woods-Saxon, and density-dependent folding with imaginary Woods-Saxon optical model calculations, respectively. The optical model parameters used in the calculations are given in Table I. All calculations are angle-weighted-average cross sections and are plotted versus average center-of-mass angle.

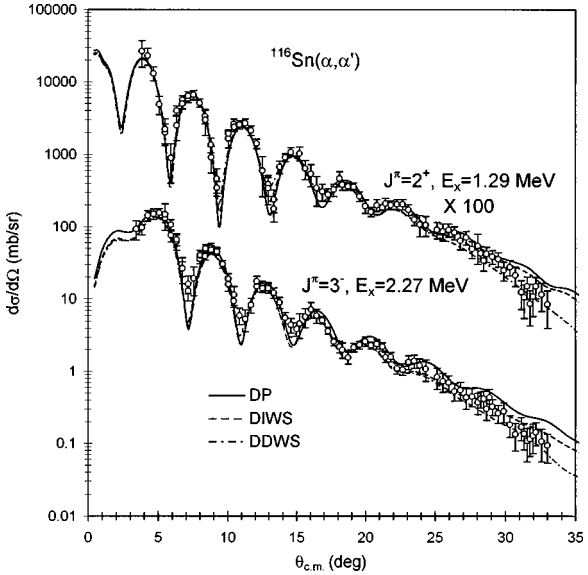

FIG. 2. Inelastic scattering differential cross sections obtained for states indicated of ^{116}Sn excited by 240 MeV α particles plotted versus average center-of-mass angle. The error bars represent the combined uncertainty from statistical and systematic error summed in quadrature. The solid, dashed, and dashed-dot lines are DWBA calculations made with deformed potential, density-independent folding with imaginary deformed potential, and density-dependent folding with imaginary deformed potential transition models, respectively. Each calculation used the electromagnetic value for the transition rate $B(E2)=0.229\ e^2\ \mathrm{b}^2$ which corresponds to a deformation length of $\delta_2=0.680$ fm and $B(E3)=0.120\ e^2\ \mathrm{b}^3$ which corresponds to a deformation length of $\delta_3=0.815$ fm. All calculations are angle-weighted-average cross sections and are plotted versus average center-of-mass angle.

tegration and were read in as input. For all the calculations, PTOLEMY determined the Coulomb potential by double folding over the charge distributions of the target and projectile with radii determined by $R_t^c=1.2074\times M_t^{1/3}$ and $R_p^c=1.3342\times M_p^{1/3}$, where M_t and M_p are the target and projectile masses.

Optical model parameters were determined for the elastic scattering data using the fitting routine of PTOLEMY. PTOLEMY cannot properly average the calculated cross section over our experimental solid angle, however, for $\theta_{\mathrm{lab}}=2.5°$ the effect is less than 1% except in the deep minima. Therefore, experimental data points below 2.5° were not included in the fits. Real and imaginary volume integrals were determined by the relation

$$J_{V,W}=\frac{1}{A_T A_p}\int V(r),W(r)d\tau, \tag{10}$$

where $V(r)$ and $W(r)$ are the real and imaginary parts of the optical model and A_T and A_p are the nucleon numbers of the target and projectile.

The CWS, DIWS, and DDWS optical models were fit to the data and the parameters obtained are listed in Table I. The χ^2 values of the fits are 1.5, 1.9, and 1.8, respectively. The parameters obtained with the CWS model are very close to those from Ref. [17] who measured elastic scattering of 288 MeV α particles out to $\theta_{\mathrm{c.m.}}\sim 32°$. The different real and imaginary radial parameters obtained with the CWS model illustrate the need for the different radial expression for the imaginary part of the folding model. The volume integrals obtained with each model are also listed in Table I. The values obtained with the DDWS model are about 5% lower than those from the CWS optical model and are about 30% lower than those from the DIWS optical model. The large difference between folding models results from density dependence, however, both folding models fit the data equally well. The calculated angular distributions obtained with each

TABLE I. Optical model parameters obtained from fits to elastic scattering data using different models: complex Woods-Saxon, density-independent folding with imaginary Woods-Saxon, and density-dependent folding with imaginary Woods-Saxon. Volume integrals are also shown.

Model	v (MeV)	V (MeV)	R_v (fm)	a_v (fm)	J_v (MeV fm^3)	W (MeV)	R_w (fm)	a_w (fm)	J_w (MeV fm^3)
CWS		88.6	6.01	0.747	200	23.3	6.93	0.837	80
DIWS	23.12				235	42.8	5.98	0.918	102
DDWS	36.7				190	23.9	6.45	1.05	73

TABLE II. Transition rates and deformation lengths for the low-lying states and sum rule percentages for the HEOR of ^{116}Sn obtained by using different models: deformed potential, density-independent folding with imaginary deformed potential, and density-dependent folding with imaginary deformed potential. EM denotes an electromagnetic measurement. The values quoted for Ref. [14] were obtained from their data with the method described in the text.

		$J^\pi=2^+$, $E_x=1.28$ MeV		$J^\pi=3^-$, $E_x=2.29$ MeV		HEOR
work	model	$B(E2)$ (e^2 b^2)	δ_2(fm)	$B(E3)$ (e^2 b^3)	δ_3(fm)	%$E3$ EWSR
present	DP	0.231 ± 0.023	0.683 ± 0.035	0.114 ± 0.012	0.794 ± 0.043	70 ± 15
present	DIWS	0.231 ± 0.023	0.683 ± 0.035	0.134 ± 0.014	0.861 ± 0.046	83 ± 15
present	DDWS	0.231 ± 0.023	0.683 ± 0.035	0.134 ± 0.014	0.861 ± 0.046	83 ± 15
Refs. [18,19]	EM	0.229 ± 0.015	0.680 ± 0.023	0.120 ± 0.015	0.815 ± 0.053	
Ref. [14]	DP			0.118 ± 0.012	0.808 ± 0.040	
Ref. [1]	DP					67 ± 10

model are shown by the solid, dashed, and dashed-dotted lines in Fig. 1.

Using the optical-model parameters in Table I, coupled-channel distorted-wave Born approximation (DWBA) calculations were carried out with PTOLEMY for the HEOR and the low-lying states. Following the relations of Eqs. (8) and (9), EWSR percentages, transition rates, and deformation lengths were determined from the fits of the calculated angular distributions to the data. The values for $\langle r\rangle$, $\langle r^2\rangle$, and $\langle r^4\rangle$, calculated numerically, are 4.420 fm, 21.38 fm^2, and 602.4 fm^4, respectively.

The electromagnetic transition rates for the low-lying 2^+ and 3^- states of ^{116}Sn are $B(E2)=0.229\pm0.015\ e^2$ b^2 [18] and $B(E3)=0.120\pm0.015\ e^2$ b^3 [19] and the corresponding deformation lengths are $\delta_2=0.680\pm0.023$ fm and $\delta_3=0.815\pm0.053$ fm. Figure 2 shows the angular distributions calculated using the DP, DIWS, and DDWS models using these values superimposed on the data. For the 2^+ state, the integrated differential cross sections (over $3°\leqslant\theta_{\rm c.m.}\leqslant33°$) obtained from the three calculations agree to within 1%, and fit the data well at small angles. The DP, DIWS, and DDWS model calculations fit the entire data range with χ^2 values of 2.2, 1.8, and 1.3, respectively. For the 3^- state, the angular distributions obtained with the DDWS and DIWS models fit the phase and magnitude of the data well (with χ^2 values of 1.2 for both) and their integrated differential cross sections agree to within 1%. The calculated angular distribution with the DP model follows the phase of data well (with a χ^2 value of 1.9) and the magnitude is only slightly too high. The integrated differential cross section using the DP model is $\sim$18% higher than that obtained with the folding models. The transition rates and deformation lengths required to fit the data are listed in Table II, and the values are in agreement, within the uncertainty, of the values from electron scattering [18,19].

For a HEOR which exhausts the full $E3$ EWSR at $E_x=21.8$ MeV, the deformation length would be $\delta_3=0.894$ fm and the transition rate would be $B(E3)=0.144\ e^2$ b^3. Differential cross sections obtained with the DDWS and DIWS models agree at the first maximum to within 1% while the cross section obtained with the DP model is $\sim$18% higher. These are consistent with the results found for the low-lying 3^- state. Figure 3 shows the angular distributions calculated with the DP, DIWS, and DDWS models normalized to the data. They correspond to 70, 83, and 83 % of the $E3$ EWSR, respectively. The data points are taken from Ref. [1] and the error bars represent the combined uncertainty from statistical and systematic error summed in quadrature. The sum rule percentages obtained with each model and uncertainties are listed in Table II. The 15% errors are associated only with the uncertainty of the cross section of the HEOR. Cross sections obtained in the first maximum for the HEOR with different families of potentials (which fit the elastic data within $\chi^2<4$) were found to differ by less than 1% for all models. The result obtained here with the DP model is in agreement with 67% of the $E3$ EWSR presented in our initial work [1].

VI. CONCLUSION

We have studied the effect of using a DP model and single folding models with and without density dependence

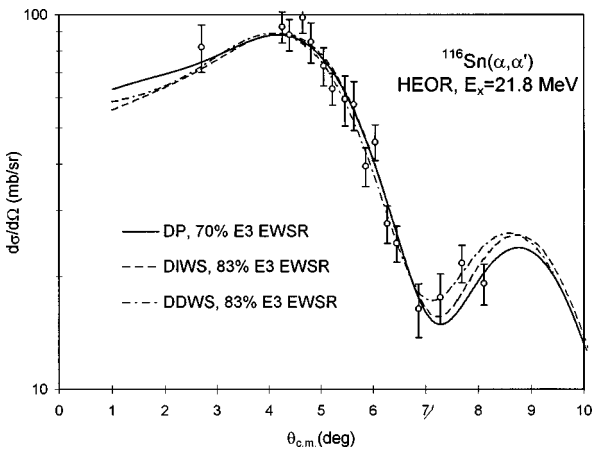

FIG. 3. Angular distribution of the differential cross section obtained from Ref. [1] for the $E_x=21.8$ MeV HEOR of ^{116}Sn excited by 240 MeV α particles plotted versus average center-of-mass angle. The error bars represent the combined uncertainty from statistical and systematic error summed in quadrature. The solid, dashed, and dashed-dot lines are DWBA calculations made with deformed potential, density-independent folding with imaginary deformed potential, and density-dependent folding with imaginary deformed potential models, respectively, normalized to 70, 83, and 83 % of the $E3$ EWSR. Each calculation has been angle-weighted averaged over the bin width $\Delta\theta=0.4°$ and vertical spectrometer acceptance $\Delta\phi=4.0°$ and are plotted versus average center-of-mass angle.

to obtain the sum rule strength of the HEOR and the transition rates of the low-lying 2^+ and 3^- states of ^{116}Sn excited by 240 MeV α scattering. Octupole transition rates obtained with density dependent and density independent folding are essentially identical, and both are about 18% higher than these obtained with the deformed potentials. Quadrupole transition rates obtained with all these models agree within 1%. The transition rates obtained for the low-lying states of ^{116}Sn with all these models agree, within the uncertainty, with electromagnetic values. For the HEOR, we obtained strengths of 70 and 83 % of the $E3$ EWSR with DP and folding model analyses, respectively. These results are both consistent with the expectation that the HEOR of ^{116}Sn should exhaust approximately $\frac{2}{3}$ of the $E3$ EWSR [1].

ACKNOWLEDGMENTS

This work was supported in part by the U.S. Department of Energy under Grant No. DE-FG03-93ER40773 and by The Robert A. Welch Foundation.

[1] H. L. Clark, D. H. Youngblood, and Y.-W. Lui, Phys. Rev. C **54**, 72 (1996).
[2] J. R. Beene, D. J. Horen, and G. R. Satchler, Phys. Lett. B **344**, 67 (1995).
[3] G. R. Satchler and Dao T. Khoa, Phys. Rev. C **55**, 285 (1997).
[4] G. R. Satchler, *Direct Nuclear Reactions* (Oxford University Press, Oxford, 1983).
[5] A. M. Bernstein, Adv. Nucl. Phys. **3**, 325 (1969).
[6] F. E. Bertrand, G. R. Satchler, D. J. Horen, J. R. Wu, A. D. Bacher, G. T. Emery, W. P. Jones, D. W. Miller, and A. van der Woude, Phys. Rev. C **22**, 1832 (1980).
[7] G. R. Satchler, Nucl. Phys. **A579**, 241 (1994).
[8] J. R. Beene, D. J. Horen, and G. R. Satchler, Nucl. Phys. **A596**, 137 (1996).
[9] E. Friedman, H. J. Gils, H. Rebel, and Z. Majka, Phys. Rev. Lett. **41**, 1220 (1978).
[10] A. Bohr and B. R. Mottelson, *Nuclear Structure* (Benjamin, Reading, MA, 1975).
[11] D. M. Pringle, W. N. Catford, J. S. Winfield, D. G. Lewis, N. A. Jelley, K. W. Allen, and J. H. Coupland, Nucl. Instrum. Methods Phys. Res. A **245**, 230 (1986).
[12] D. H. Youngblood and J. Bronson, Nucl. Instrum. Methods Phys. Res. A **361**, 37 (1995).
[13] D. H. Youngblood, Y.-W. Lui, H. L. Clark, P. Oliver, and G. Simler, Nucl. Instrum. Methods Phys. Res. A **331**, 539 (1995).
[14] H. L. Clark, Y.-W. Lui, and D. H. Youngblood, Nucl. Phys. **A589**, 416 (1995).
[15] M. Rhoades-Brown, M. H. MacFarlane, and S. C. Pieper, Phys. Rev. C **21**, 2417 (1980); **21**, 2436 (1980); M. H. MacFarlane and S. C. Pieper, Argonne National Laboratory Report No. ANL-76-11, Rev. 1, 1978.
[16] G. R. Satchler, Nucl. Phys. **A540**, 533 (1992).
[17] B. Bonin, N. Alamanos, B. Berthier, G. Bruge, H. Faraggi, J. C. Lugol, W. Mittig, L. Papineau, A. I. Yavin, J. Arviex, L. Farvacque, M. Buenard, and W. Bauhoff, Nucl. Phys. **A445**, 381 (1985).
[18] J. W. Lightbody, S. Penner, S. P. Fivozinsky, P. L. Hallowell, and H. Crannen, Phys. Rev. C **14**, 952 (1976).
[19] P. Barreau and J. B. Bellicard, Phys. Rev. Lett. **19**, 1444 (1976).